Wet-type Packed-bed Nonthermal Plasma for Simultaneous Removal of PM and VOCs*

Takumi Shimada[1], Haruhiko Yamasaki[1, 2], Tomoyuki Kuroki[1, 2], Jinkyu Kang[3], Dong-Wook Kim[3], Tadao Yagi[4], and Masaaki Okubo[1, 2]

[1] Department of Mechanical Engineering, Osaka Prefecture University, 1-1 Gakuen-cho, Naka-ku, Sakai 599-8531, Japan

[2] Department of Mechanical Engineering, Osaka Metropolitan University, 1-1 Gakuen-cho, Naka-ku, Sakai 599-8531, Japan

[3] Samsung Advanced Institute of Technology, Samsung Electronics Co., Ltd., 130 Samsung-ro, Yeongtong-gu, Suwon-si, Gyeonggi-do, 16678, Korea

[4] Samsung Device Solutions R&D Japan, Samsung Japan Corporation, 2-7 Sugasawa-cho, Tsurumi-ku, Yokohama 230-0027, Japan

*The final publication of this paper is

Shimada, T., Yamasaki, H., Kuroki, T. Kang, J., Kim, D-W., Yagi, T., Okubo, M., Wet-Type Packed-Bed Nonthermal Plasma for Simultaneous Removal of PM and VOCs. Plasma Chem Plasma Process (2023). https://doi.org/10.1007/s11090-023-10403-1

Abstract Several regulations on exhaust gases have been introduced to curb hazardous exhaust of volatile organic compounds (VOCs) and particulate matter (PM) from the paint and printing industries. VOCs produce photochemical oxidants and suspended PM such as $PM_{2.5}$, which is now recognized as a global environmental problem. We assess a nonthermal plasma (NTP) technique for controlling VOC emissions, especially, propose a wet-type packed-bed plasma reactor to extend the treatment of water-non-soluble VOCs. This paper proposes a wet-type packed-bed plasma reactor to extend the treatment of water-non-soluble VOCs. The proposed technique is evaluated through the simultaneous removal of nanoparticles and toluene at a relatively high flow rate. Simultaneous treatment of the VOCs and nanoparticles using the reactor indicates that the average particle collection efficiency is 94%, and the removal efficiency of 60 ppm toluene is 73% with a gas flow rate of 10 L/min. The resultant byproducts are benzaldehyde (C_6H_5CHO), benzyl alcohol ($C_6H_5CH_2OH$), phenol (C_6H_5OH), ozone, formic acid, and acetic acid, and some are easily dissolved and removed by the sodium hydroxide solution film. A smaller pellet diameter leads to more efficient toluene removal at lower specific energy values, while the ozone concentration does not change. However, the ozone concentration can be greatly suppressed by dissolving the ozone in the alkali solution film.

Keywords: Nonthermal plasma, volatile organic compounds, particulate matter, wet-type, NaOH solution

Masaaki Okubo (email corresponding author)

Department of Mechanical Engineering, Osaka Metropolitan University, 1-1 Gakuen-cho, Naka-ku, Sakai 599-8531, Japan

e-mail address: mokubo@mokubo.com

Introduction

Air contaminants, such as volatile organic compounds (VOCs) and tiny airborne particles, have become societal concerns. Rules concerning emission controls, including those for ships, have been established. The paint and printing sectors release exhaust fumes that contain VOCs, which lead to the creation of photochemical pollutants and particulate matter (PM), such as $PM_{2.5}$, posing a worldwide environmental threat. Furthermore, VOCs pose health risks because of their potential to cause cancer. Specifically, they have been identified as the factor causing sick building syndrome. Hence, innovative methods are required to prevent their release into the air [1].

Traditional methods to capture VOCs include techniques based on photo- and thermal catalytic removal [2–4], adsorbent usage [5], and biofiltering [6]. Thermo catalytic combustion is noteworthy because it occurs at low temperatures. However, this needs the use of valuable metals such as Pt and Pd, raising the overall expense. In addition, standard methods face challenges in minimizing and eliminating VOCs owing to their significant energy consumption and incapacity to handle shifts in gas flow speeds. Therefore, there is a need for efficient and affordable solutions for removing VOCs gases. The nonthermal plasma (NTP) method [7–13] eliminates many harmful air contaminants more effectively than traditional methods. This approach offers unique benefits, such as

no maintenance, reduced operation expenses, and extensive usability under ambient temperature and pressure conditions. Nevertheless, the use of NTP in managing VOCs is constrained by its inferior energy productivity and the generation of unwanted byproducts such as ozone (O_3), nitrogen oxides (NO_x), and VOC agglomerated nanoparticles. Therefore, the present study focuses on the efficient removal of VOCs and suppressing the undesirable byproducts by combining NTP with chemicals, materials, and the sodium hydroxide (NaOH) solution as a system.

Packed-bed plasma reactors are used for odor and VOC removal [14–21]. The most widely known effect of packing materials is electric-field augmentation at the contact point between the pellets [21]. Additionally, scientists have investigated the elimination of VOCs using nonthermal plasma reactors containing pellets [22]. The wet variant demonstrated superior efficiency compared to the dry variant. Moreover, VOCs are converted into by-products that are soluble in water, which enhances the effectiveness of these methods for treating gases. Ozone emission from plasma air cleaners has become a problem because they are harmful to humans. It is reported that the ozone is decomposed by an NaOH solution. The autolysis reaction of the ozone is initiated by hydroxide ion (OH^-) when the aqueous solution is alkaline [23]. Manganese oxide is used to control ozone in a packed-bed plasma reactor, which requires maintenance, such as replacing

manganese oxide because of its limited lifetime [1]. Moreover, if the catalyst is placed after the plasma reactor, more of it is required to eliminate ozone when the gas flow rate is higher. Thus, the NaOH solution film can be used to reduce ozone without a catalyst, which facilitates maintenance. Furthermore, it has been reported that NO_x and nitric acid (HNO_3) in the plasma can be neutralized by the NaOH solution film [11]. Additionally, Carbon dioxide (CO_2) produced by the decomposition of toluene ($C_6H_5CH_3$) can also be absorbed by the NaOH solution film under alkaline conditions [11]. One of the properties of packing materials that affects the discharge is the pellet size [24, 25]. By reducing the diameter of the pellets in the filling layer, the number of contact points and the total surface area of the pellets are increased. Thus, the energy efficiency of the discharge on the sphere surface is increased, and the efficiency of VOC removal is considered to increase [25].

Given the aforementioned context, we propose using a wet-type packed-bed NTP method for removing VOCs. The benefits of this method include superior energy efficiency, use of highly chemically active agents such as oxygen and hydroxyl radicals (•O and •OH), transformation to water-soluble products, and gathering of nanoparticles. In the present study, we evaluated the performance of the proposed plasma reactor through the simultaneous removal of nanoparticles and one of the typical VOCs, e.g.,

toluene, at a relatively high gas flow rate of 10 L/min. A detailed analysis of reaction byproducts is performed compared with the dry-type packed-bed NTP reactor.

Principle of Simultaneous Removal

Wet-type Packed-bed NTP Reactor

Figure 1 shows a schematic of the wet-type packed-bed NTP reactor used in the experiment. An overview of the reactor is displayed on the right side of the figure, and a detailed depiction of the plasma region is shown on the left. The reactor consists of a quartz tube, stainless-steel wire (serving as the discharge electrode), silver paste (acting as the grounded electrode), glass pellets, tank for overflow, bottom tank, storage tank, pump for the liquid, and a flow meter device. The quartz tube, positioned vertically, is a round tube with an inner diameter of 20 mm, an outer diameter of 25 mm, and a length of 646 mm; its exterior is coated with a silver paste adhesive up to 260 mm high and is 0.05 mm thick. The discharge electrode strand measuring 2.0 mm in diameter is positioned along the center of the quartz tube. The glass pellets with diameters of 2.0 ± 0.5 mm are packed in the quartz tube in the section painted with the silver paste. Glass is used as a typical dielectric pellet. Subsequently, NaOH solution passed from an overflow tank above the quartz tube flows along the tube's inner wall to create a solution film. NTP

is produced by delivering a high-voltage pulse to the discharge electrode. Owing to the hydrophilic inner surface established by NTP, the solution film moves consistently along the inner lining of the tube and pellets. This mechanism increases the contact area between the gas and liquid. Because the gas and the solution film are more likely to come into contact with each other, the ozone dissolves in the solution film, and the ozone concentration is reduced compared with a wet-type NTP reactor without pellets.

The close-up perspective of the plasma region in **Fig. 1** reveals that the PM acquires a positive charge when it encounters the electric field created by the discharge electrode and then moves towards the ground electrode. The interior surface of the tube along with the ground electrode neutralizes the charged particles, and the nanoparticles are transported downstream inside the solution film. Subsequently, the gaseous air contaminants traveling through the channel are isolated for further processing. The fluid that traversed the quartz tube is collected in the bottom tank which is then moved to the overflow tank for circulation during the tests.

Chemical Reactions for Toluene Decomposition

Toluene decomposition using the wet-type nonthermal plasma reactor occurs owing to two processes: ring-opening reactions by high-speed electrons and oxidative

decomposition reactions by active species and radicals. For oxidative decomposition, the possible chemical reactions that produce active species such as oxygen, hydroxyl, hydroperoxyl radicals, superoxide anion, and ozone are mainly shown in reactions (1)–(17) [26–35].

$$H_2O + e^- \rightarrow e^- + \bullet OH + \bullet H \quad (1)$$

$$O_2 + e^- \rightarrow \bullet O + \bullet O + e^- \quad (2)$$

$$\bullet O + H_2O \rightarrow \bullet OH + \bullet OH \quad (3)$$

$$O_2 + \bullet O + M \rightarrow O_3 + M \quad (4)$$

$$O_3 + H_2O \rightarrow O_2 + \bullet OH + \bullet OH \quad (5)$$

$$\bullet OH + \bullet OH \Leftrightarrow H_2O_2 \quad (6)$$

$$H_2O_2 + 2OH^- \rightarrow \bullet O_2^- + 2H_2O + e^- \text{ (for high pH)} \quad (7)$$

$$H_2O_2 + \bullet O_2^- \rightarrow O_2 + \bullet OH + OH^- \quad (8)$$

$$O_3 + \bullet O_2^- \rightarrow \bullet O_3^- + O_2 \quad (9)$$

$$\bullet O_2^- + H^+ \rightarrow HO_2\bullet \quad (10)$$

$$HO_2\bullet \rightarrow \bullet OH + O_2 \quad (11)$$

$$H_2O_2 \Leftrightarrow H^+ + HO_2^- \quad (12)$$

$$O_3 + HO_2^- \rightarrow \bullet OH + O_2 + \bullet O_2^- \quad (13)$$

$C_6H_5CH_3 + \bullet O, \bullet OH, \bullet O_2^-, HO_2\bullet \rightarrow$ Intermediates (14)

Intermediates + $\bullet O, \bullet OH, \bullet O_2^-, HO_2\bullet \rightarrow CO_2 + H_2O$ (15)

$C_6H_5CH_3 + e^- \rightarrow$ Intermediates (16)

Intermediates + $e^- \rightarrow CO_2 + H_2O$ (17)

According to reaction (1), hydroxyl radical (•OH) is generated via the collisions of electrons with water molecules induced by discharge. Reaction (2) indicates that oxygen radicals (•O) are generated as a result of electron collisions with oxygen molecules, and reaction (3) illustrates that hydroxyl radicals are generated when oxygen radicals react with water molecules. The plasma generates O_3 by reaction (4). As shown in reaction (5), •OH is generated by the reactions between plasma-generated O_3 in the gas phase, UV radiation, and water molecules. As shown in reaction (6), hydrogen peroxide (H_2O_2) is generated when excess hydroxyl radicals are present, but it is again degraded to hydroxyl radicals such as by the plasma-based UV rays. Furthermore, as shown in Reactions (7)–(13), oxygen, hydroxyl, and hydroperoxyl ($HO_2\bullet$) radicals and superoxide anion ($\bullet O_2^-$) are generated from various reactions related to H_2O_2 and O_3. As shown in reactions (14) and (15), toluene ($C_6H_5CH_3$) reacts with the radicals to generate intermediates such as benzyl radical ($C_6H_5CH_2\bullet$) benzaldehyde (C_6H_5CHO), benzyl alcohol ($C_6H_5CH_2OH$),

phenol (C_6H_5OH), formic acid (HCOOH), acetic acid (CH_3COOH), etc., which ultimately degrade to carbon dioxide and water. Toluene is also decomposed by a ring-opening reaction with high-speed electrons e^- induced by the plasma in reaction (16). Toluene ultimately degrades to carbon dioxide and water in reaction (17). Water-soluble gas phase byproducts of HCOOH and CH_3COOH react with NaOH in the solution film.

$$HCOOH + NaOH \rightarrow HCOONa + H_2O \quad (18)$$

$$CH_3COOH + NaOH \rightarrow CH_3COONa + H_2O \quad (19)$$

It is noted that nitric oxide (NO), nitrogen dioxide (NO_2), nitrous acid (HNO_2), HNO_3, and nitrous oxide (N_2O) are induced in the wet-type NTP reactor [12]. However, the concentrations of them are too low to be detected in the present experiment. When a small amount of NO_2, HNO_2, and HNO_3 is induced, it can be absorbed and neutralized by the NaOH solution film in the wet-type NTP reactor.

Experimental Apparatus and Method

Figure 2 shows a schematic of the experimental setup. Gas generators and tanks are employed to create synthetic exhaust gases at rates of either 8 or 10 L/min with toluene.

Toluene with a purity of 99.5% is vaporized in two of these devices, and a mixture of air (O_2 at 21% and N_2 at 79%) is introduced to simulate exhaust gases with VOCs. Concurrent PM processing is initiated using an aerosol made by directing air at a flow rate of 2 L/min through an aerosol generator (Model 3076, TSI Inc.). This device holds a mixture of polystyrene latex (PSL) particles with six different mean diameters: 29, 47, 61, 100, 202, and 303 nm (SC-0030-A, SC-0051-D, SC-0060-D, and SC-024-S for sizes 29, 47, 61, and 202 nm from JSR Co.; and 3100A and 3300A for 100 and 303 nm from Thermo Fisher Scientific Co., Ltd.). Toluene is vaporized through gas generators (PERMEATER PD-1B-2, Gastec Co.) and mixed with the aerosol. The mixed gas is then transferred to the reactor at a flow rate of 10 L/min. The output of the extraction air pump located after the reactor is modified to achieve an inlet pressure of approximately 0.01 MPa. Furthermore, when measuring the concentration of particles with a diameter of 400 nm or larger, toluene is generated at a flow rate of 0.5 L/min using a gas generator and a gas cylinder and mixed with 9.5 L/min of the synthesized air for a total of 10 L/min of mixed gas pumped into the reactor. We feed the gas mixture in the wet-type packed-bed reactor through an inlet at the top and release it through an outlet at the bottom. Tap water forming at the bottom tank is funneled back to the top of the reactor for circulation. A high-voltage pulse with a pulse frequency of 210 or 840 Hz is applied to the discharge

electrode in the reactor to generate NTP. The instant patterns of the applied voltage, current, and time-dependent power are recorded using a voltage *V* probe (P6015A, conversion ratio = 1 kV/V, Tektronix Inc.), current *I* probe (P6021, conversion ratio = 10 A/V, Tektronix Inc.), and a digital scope (DLM2054, Yokogawa Electric Co.), respectively. The packed-bed plasma reactor is filled with spherical glass pellets. The gas is sampled before and after the reactor and stored in a gas-sampling bag for later examination. The concentrations of toluene and ozone are determined using a gas detection tube (122 L for toluene and 18M for ozone, Gastec Co.), gas analysis machine (GC-14B, Shimadzu Corporation), and ozone analysis machine (PG-621MA-G, Ebara Jitsugyo Co., Ltd.). Aerosol is examined with a scanning mobility particle sizer (SMPS) (differential mobility analyzer (DMA): Model 3080 + condensation particle counter (CPC): Model 3787, particle size measurement span:10 to 414 nm, TSI Inc.) and laser particle counter (LPC, light scattering method, false count = 1 or less per 5 min, accidental counting error = 10% or less, 140,000,000 counts per m^3, Met One particle counter HHPC3+, Beckman Coulter, Inc.) after ozone elimination with a tubular heater (KRO-14K, Isuzu Seisakusho Co., Ltd.) set at 250 °C located after the reactor. Byproducts are analyzed using Fourier transform infrared spectroscopy (FTIR, IRTracer-100, Shimadzu Corporation). The FTIR measurement conditions are as follows: box-car apodization

function, 20 integrations, a resolution of 0.5 cm^{-1}, and a wavenumber range of 1000–4000 cm^{-1}. A gas cell (PIKE Technologies, Inc.) with an optical path length of 2.4 m, a volume of 0.1 L, a window material of CaF_2, a window diameter of 25 mm, and a thickness of 4 mm is used. The gas cell is heated at 100 °C and passed through a drain pot and polytetrafluoroethylene (PTFE) filter (AS ONE Co., FPT502020Y, diameter = 50 mm, pore size = 0.2 μm) installed downstream of the reactor to remove water and particles. Byproducts are determined using the National Institute of Advanced Industrial Science and Technology (NIST) database [36] and the Spectral Database of Organic Compounds [37].

Experimental Results and Discussion

Voltage and Current Waveforms

Figure 3 shows the typical waveforms of the voltage V, current I, and instantaneous power $V \times I$ for the plasma reactor. A pulse dielectric barrier discharge (DBD) is induced in the reactor. The power P averaged over time is determined by integrating the instantaneous power of the positive region throughout a single cycle and then multiplying it by the pulse frequency f and the conversion factors of the current and voltage probes. As shown in the figure, the time-averaged discharge power of the air plasma is 41 W at

an applied peak voltage of 23 kV, pulse frequency of f = 840 Hz, and NaOH solution concentration of 2.5 mmol/L. The wet-type packed-bed NTP reactor exhibits a relatively large peak current exceeding 17 A, whereas the dry-type NTP reactor usually exhibits less than 10 A peak.

Particle Concentration and Partial Collection Efficiency

Figure 4 shows the typical particle-size distribution of nanoparticles introduced into the reactor at the inlet without solution flow and plasma application. The measurement is performed for 10 min. The result corresponds to the case without solution flow and plasma application. The vertical axis shows the adjusted concentration dN/dlogD_p, with units in #/cm^3. In the figure, # signifies the particle count and D_p represents the electrical mobility or Stokes diameter of an individual particle. The error bars shown in the figure are based on the standard deviation of three measurements. To evaluate the normalized particle number concentration using SMPS, a blend of air with PSL particles (sizes ranging from 20 to 334 nm) and toluene is used. For larger particle sizes, LPC is used to measure the concentration of particles at 300, 500, 1000, 2000, and 5000 nm in a mixture of room air and toluene. The normalized particle number concentrations at 400, 750, 1500, and 3500 nm are then determined using the following formula:

$$\frac{\mathrm{d}N}{\mathrm{d}\log_{10} D_\mathrm{p}} = \frac{N_\mathrm{b} - N_\mathrm{a}}{\log_{10} D_\mathrm{a} - \log_{10} D_\mathrm{b}} \tag{20}$$

where D_a and D_b represent two particle sizes (nm) and N_a and N_b represent the concentrations (#/cm^3) of particles larger than D_a and D_b, respectively, as measured using LPC. The combinations of D_a and D_b (nm) are (D_a, D_b) = (300, 500), (500, 1000), (1000, 2000), and (2000, 5000). This figure confirms that the particle size distribution matches the diameters of the six distinct polystyrene particles.

Figure 5 shows the size-dependent partial collection efficiency for nanoparticles in the diameter range of 20–3500 nm and at an NaOH solution flow rate of q = 75 mL/min with plasma application. The pulse frequency is set to f = 840 Hz with a solution flow rate of q = 75 mL/min, NaOH solution concentration of 2.5 mmol/L, pH of 11, conductivity of 59 mS/m, and gas flow rate of Q = 10 L/min. The applied peak voltage is varied. The concentrations are measured using SMPS three times, each lasting for 2 min. The figure shows the average particle collection efficiencies at each of the three applied peak voltages of 18, 20, and 22 kV. The average collection efficiency in the particle-size range is 83% at 18 kV, 92% at 20 kV, and 94% at 22 kV. The collection efficiency increases with the applied peak voltage. However, in the measurement range of the SMPS, the

collection efficiency decreases with an increase in the particle size, owing to a measurement error caused by the lower inlet particle number concentration. The collection efficiency for room air and toluene stream with the LPC measurement is the highest at 400 nm because the calculated particle number concentration at 400 nm for room air and toluene stream is 230 #/cm^3, which is approximately 100 #/cm^3 higher than that at 333.8 nm with PSL particles and toluene stream with the SMPS measurement. Owing to the higher particle number concentration at 400 nm, the particle collection efficiency is highest at 400 nm. The concentration at 750 nm is 13.2 #/cm^3, that at 1500 nm is 1.83 #/cm^3, and that at 3500 nm is 0.424 #/cm^3. These results indicate that during the experiment, more particles with sizes of approximately 400 nm exist in the room air: therefore, the removal efficiency becomes highest at 400 nm.

Toluene Removal Efficiencies and Ozone Concentration

Figure 6 shows the relationship between the toluene removal efficiency and the specific energy (*SE*) with various solution flow rates, NaOH solution concentrations, and initial concentrations at a pulse frequency of f = 840 Hz with a gas flow rate of Q = 10 L/min. The inlet concentration of toluene ranges from 20 to 36 ppm. The toluene removal efficiency decreases by 13% when the NaOH solution concentration is increased from 2.5

to 6.25 mmol/L, because the amount of power required for plasma generation increases as the NaOH solution concentration increases. In addition, the increase in the NaOH solution concentration increases the current value and decreases the electric-field strength, which suppresses the decomposition of toluene by electron collision. Conversely, the toluene removal efficiency is increased when the NaOH solution concentration is increased from 0.31 to 0.63 mmol/L. This is possible because the conductivity increases from 7 to 14 mS/m, and the discharge stabilizes. Furthermore, for the same NaOH solution concentration, the average toluene removal efficiency increases slightly with an increase in the solution film flow rate. The toluene removal efficiency at $SE = 0$ increases with an increase in the initial toluene concentration. This is possibly due to the reason that toluene gas flows into the NaOH solution film, and inducing a gas-liquid two-phase flow. As a result, the toluene is transported, and its concentration is reduced upon exiting the reactor. In a wet-type packed-bed plasma reactor, a maximum toluene removal efficiency of 73% is achieved at an NaOH solution concentration of 2.5 mmol/L and a solution film flow rate of 75 mL/min. The maximum toluene removal efficiency is 10% higher than the toluene removal efficiency of 63% with an NaOH solution concentration of 0 mmol/L and a solution film flow rate of 100 mL/min. Furthermore, the maximum toluene removal efficiency is similar to the toluene removal efficiency of 74% at a solution film flow rate

of 0 mL/min. In these results, the best toluene removal efficiency for lower *SE* is obtained in the case without water solution film. This is caused by the increase in discharge current due to the flow of the solution. Consequently, both the discharge power and *SE* become larger for the removal efficiency in the case with water solution film. In **Fig. 6**, to achieve a removal efficiency of approximately 73%, the discharge power is 14 W at q = 0 mL/min while it is 47 W at NaOH concentration = 0.63 mmol/L and q = 100 mL/min. *SE* becomes approximately 3.4 times larger with the flow of the water solution.

Figure 7 shows the relationship between the concentration of ozone at the reactor outlet and *SE* with various solution flow rates, NaOH solution concentrations, and initial toluene concentrations at a pulse frequency of f = 840 Hz and a gas flow rate of Q = 10 L/min. Compared with a solution film flow rate of q = 0 mL/min, the ozone concentration is reduced by 97 ppm to 76 ppm at a solution film flow rate of q = 100 mL/min and NaOH solution concentration of 0 mmol/L. Furthermore, when the solution film flow rate is q = 100 mL/min, and the NaOH solution concentration is 2.5 mmol/L, the ozone concentration is reduced by 42 ppm to 34 ppm. For the same NaOH solution concentration, the ozone concentration decreases as the solution film flow rate increases. As an example, when the NaOH solution concentration is 2.5 mmol/L, and the solution film flow rate is increased from q = 50 mL/min to q = 100 mL/min, the ozone concentration decreases by

26 ppm. For the same solution film flow rate, the ozone concentration decreases with an increase in the NaOH solution concentration. As an example, when the solution film flow rate increases to q = 100 mL/min and the NaOH solution concentration increases from 0.31 to 6.25 mmol/L, the ozone concentration decreases by approximately 100 ppm, because ozone not only dissolves in the water film but also reacts with OH^- in the following reaction, and the ozone can be reduced [23, 38].

$$O_3 + OH^- \rightarrow HO_2^- + O_2 \quad (21)$$

The NaOH solution film can absorb ozone far better than the water film under pH > 8 or an alkali condition [23, 38]. Note that the following reaction (22) is a fast process and is important for waters with low scavenger concentrations or low alkalinity, it leads to the consumption of ozone and •OH and lowers the oxidation capacity in the system [23].

$$O_3 + \bullet OH \rightarrow HO_2\bullet + O_2 \quad (22)$$

Byproduct Analysis and Toluene Removal Efficiency

Figure 8 shows the FTIR spectra of the byproducts with various NaOH solution

concentrations at a pulse frequency of f = 840 Hz with a solution flow rate of q = 100 mL/min and gas flow rate of Q = 10 L/min. The inlet concentration of toluene is 60 ppm. When the inlet toluene concentration was 20 ppm, small decomposition byproduct peaks appeared in the FTIR spectra, and they were too small, indicating an increase in the toluene inlet concentration. In **Figs. 8**(a)–(d), the peaks of C_6H_5CHO (1703 cm^{-1}), $C_6H_5CH_2OH$ (1020 cm^{-1}), and C_6H_5OH (1530 cm^{-1}), which are organic intermediates in reactions (14)–(17) byproducts that are not very soluble in the water film, are detected at NaOH solution concentrations of 0–6.25 mmol/L. Other peaks of $C_6H_5CH_3$ (2035 cm^{-1}, 3041 cm^{-1}), H_2O (1300–2000 cm^{-1}, 3400–4000 cm^{-1}), CO_2 (2337cm^{-1}, 2360 cm^{-1}), CO (2106 cm^{-1}, 2180 cm^{-1}), and O_3 (1050 cm^{-1}) are detected. In a dry-type packed-bed NTP reactor, organic intermediates or byproducts such as HCOOH, CH_3COOH, and C_6H_5CHO are generated [32–34]. In the wet-type packed-bed NTP reactor, HCOOH and CH_3COOH are water-soluble and are absorbed by the solution film. In addition, NO, NO_2, and N_2O peaks are not detected under any of the conditions. In the figure, the negative absorbance by water, etc., indicates that the absorbance of the sample gas is lower than that of the background gas. It is known that negative absorbance tends to appear when the optical path length of the gas cell in the FTIR system is long (2.4 m) and the N_2 purge is incomplete during measurement.

Figure 8(a) depicts the results for NaOH = 0, where toluene removal efficiency is 71%, the ozone concentration is 83 ppm, the CO_2 concentration is 36 ppm, the CO concentration is 27 ppm, the CO_2 selectivity is 12%, and the CO_x selectivity is 21%. **Fig. 8(b)** depicts the results for NaOH = 0.31 mmol/L, where toluene removal efficiency is 74%, the ozone concentration is 87 ppm, the CO_2 concentration is 18 ppm, the CO concentration is 20 ppm, the CO_2 selectivity is 6%, and the CO_x selectivity is 12%. **Fig. 8(c)** depicts the results for NaOH = 2.5 mmol/L, where toluene removal efficiency is 64%, the ozone concentration is 28 ppm, the CO_2 concentration is 13 ppm, the CO concentration is 0 ppm, and the CO_2 selectivity is 5%. **Fig. 8(d)** depicts the results for NaOH = 6.25 mmol/L, where toluene removal efficiency is 70%, the ozone concentration is 16 ppm, the CO_2 concentration is 15 ppm, the CO concentration is 0 ppm, and the CO_2 selectivity is 5%.

From these results, the CO_2 concentration decreases when the NaOH solution concentration is increased from 0 to 2.5 mmol/L. The CO_2 concentration is the lowest at the NaOH solution concentration of 2.5 mmol/L. The differences in the CO_2 concentrations for NaOH solution concentrations of 2.5 and 6.25 mmol/L are small and within the measurement error. The maximum CO_2 selectivity is as low as 12% at the NaOH solution concentration of 0 mmol/L because CO_2 is dissolved in the water film. In

addition, the CO_2 selectivity decreases with an increase in the NaOH solution concentration, because CO_2 is more soluble in the solution film. CO_2 absorption efficiency is calculated as 50–65% for NaOH concentration of 0.31–6.25 mmol/L. The CO concentration decreases when the NaOH solution concentration is increased from 0 to 2.5 mmol/L. Notably, the CO is completely removed at the NaOH solution concentrations of 2.5 and 6.25 mmol/L. This is because the CO dissolves in the NaOH solution film and does not dissolve in the water film. Therefore, the CO_2, CO, and ozone concentrations can be reduced by increasing the NaOH solution concentration. It is noted that NO_x absorption efficiency is 100% for NaOH concentration of 0.31–6.25 mmol/L.

Table 1 presents toluene removal efficiencies and O_3, CO, and CO_2 concentrations for various experimental conditions for the results in **Figs. 8(a)–(d)**. The toluene removal efficiency increases when the NaOH solution concentration is increased from 0 to 2.5 mmol/L. The toluene removal efficiency is the highest at the NaOH solution concentration of 2.5 mmol/L. The ozone concentration decreases with an increase in the NaOH solution concentration. The ozone concentration is best suppressed at the NaOH concentration of 6.25 mmol/L. It was targeted for the system that the ozone concentration is below 50 ppm. The ozone concentration is less than 50 ppm at the NaOH solution concentrations of 2.5 and 6.25 mmol/L. The optimum condition in this study is the NaOH

solution concentration of 2.5 mmol/L, which maximizes the toluene removal efficiency and minimizes the CO and CO_2 concentrations. Energy efficiency of toluene removal is estimated based on discharge power, pump power consumption (= 2.3 W for q = 100 mL/min), and NaOH power equivalent value (= 0.010 kWh/g [39]). The highest energy efficiency is calculated as 0.93 g/kWh when NaOH concentration = 2.5 mmol/L, q = 100 mL/min, removal efficiency = 72%, and discharge power = 53 W.

Effect of Pellet Size on Removal Efficiency and Ozone Concentration

Figure 9 shows the relationship between the toluene removal efficiency and *SE* with various pellet sizes at a pulse frequency of f = 210 Hz with gas flow rates of Q = 4 and 10 L/min and tap water flow rates of q = 0 and 100 mL/min. The toluene removal efficiency increases by 10% when the pellet diameter is reduced from 6.1 to 2.0 mm. The smaller pellet diameter leads to more efficient toluene removal at lower *SE* values. This is due to the increased surface area of the pellets, which increases the energy efficiency of the discharge. Additionally, the number of contact points of the pellets increases, and the strong electric field at the contact points between the pellets increases the toluene removal efficiency. In the NTP reactor without pellets, a toluene removal efficiency of 100% is achieved for water flow rates of q = 0 and 100 mL/min. However, the toluene

removal efficiency is reduced in the packed-bed NTP reactor. This is because the residence time of the gas is reduced compared with the case without pellets. The residence time or space velocity in the reactor determines the reactor efficiency. The volume of discharge without pellets is 81.7 cm^3, and filling ratio of packed pellets is assumed to be 60%. In **Fig. 9**, when 100% removal is achieved under the condition of Q = 4 L/min and q = 100 mL/min without pellets, the residence time is calculated as 1.22 s. On the other hand, under the condition of Q = 10 L/min and q = 100 mL/min with pellets, the residence time is calculated as 0.196 s. Therefore, 100% removal efficiency would be obtained if the length of the plasma reactor is made approximately 1.22/0.196 = 6.2 times longer.

Figure 10 shows the relationship between the ozone concentration and *SE* at the reactor outlet at a pulse frequency of f = 210 Hz with gas flow rates of Q = 4 and 10 L/min and tap water flow rates of q = 0 and 100 mL/min. The ozone concentration is suppressed in the presence of the water film because the ozone dissolves in the water film. The wet-type packed-bed NTP reactor can decrease 270 ppm of the ozone concentration less than the wet NTP reactor without pellets can do. In the packed-bed NTP reactor, the ozone concentration is suppressed. In addition, the ozone concentration decreases because the residence time decreases. The ozone concentration does not change when the pellet diameter is reduced from 6.1 to 2.0 mm. The contact points of the pellets increase, and

the ozone concentration increases owing to the strong electric field at the contact points between the pellets. However, the ozone concentration is suppressed by the dissolution of the ozone in the water film because the contact area between the gas and the liquid increases. Thus, the increase in the ozone concentration is offset, and the ozone concentration does not change.

Conclusions

In this study, we demonstrated the use of a wet-type packed-bed NTP reactor to simultaneously remove nanoparticles and VOCs, such as toluene. Toluene decomposition using the wet-type nonthermal plasma reactor occurs owing to two processes: ring-opening reactions by high-speed electrons and oxidative decomposition reactions by active species and radicals. The partial collection efficiency for nanoparticles is determined from the particle number concentration obtained using the SMPS and LPC. In a wet-type packed-bed plasma reactor, a maximum average collection efficiency of 94% is achieved for particle diameters in the range of 20–3500 nm, at an applied voltage of 22 kV, a gas flow rate of 10 L/min, a high-voltage pulse frequency of 840 Hz, and solution flow rate of 75 mL/min. The toluene removal efficiency decreases with an increase in the NaOH solution concentration because the amount of power required for

plasma generation increases as the NaOH solution concentration increases. In addition, the increase in the NaOH solution concentration increases the current value and decreases the electric-field strength, which suppresses the decomposition of toluene by electron collision. The resultant byproducts are benzaldehyde (C_6H_5CHO), benzyl alcohol ($C_6H_5CH_2OH$), phenol (C_6H_5OH), ozone (O_3), formic acid (HCOOH), and acetic acid (CH_3COOH), and some are easily dissolved and removed by the NaOH solution film. In a wet-type packed-bed plasma reactor, a maximum toluene removal efficiency of 73% is achieved at an NaOH solution concentration of 2.5 mmol/L, a solution film flow rate of 75 mL/min, a gas flow rate of 10 L/min, and a high-voltage pulse frequency of 840 Hz. The ozone concentration decreases with an increase in the NaOH solution concentration because ozone not only dissolves in the solution film but also is consumed by the reaction with OH^-. In a wet-type packed-bed plasma reactor, a minimum ozone concentration of 34 ppm is achieved at an NaOH solution concentration of 2.5 mmol/L and a solution film flow rate of 100 mL/min, a gas flow rate of 10 L/min, and a high-voltage pulse frequency of 840 Hz. In the wet-type packed-bed NTP reactor, water-soluble VOCs are absorbed by the solution film. In addition, the CO_2, CO, and ozone concentrations can be suppressed with an increase in the NaOH solution concentration. The CO_2 and CO concentrations are 13 and 0 ppm, respectively, at an NaOH solution concentration of 2.5 mmol/L, a solution

film flow rate of 100 mL/min, a gas flow rate of 10 L/min, and a high-voltage pulse frequency of 840 Hz. A smaller pellet diameter leads to more efficient toluene removal at lower *SE* values. This is due to the increased surface area of the pellets, which increases the energy efficiency of the discharge. The ozone concentration does not change when the pellet diameter is reduced. The ozone concentration is greatly suppressed by dissolving the ozone in the water film because the contact area between the gas and the liquid increases. Thus, the proposed wet-type NTP system addresses the global air pollution crisis by offering suppression of byproducts and cost-effective treatment for common pollutants.

Acknowledgments

The authors thank Mr. X. Xi and Mr. M. Ohashi, who are graduate students at Osaka Prefecture University, for performing the experiments.

Funding: The work was supported in part by a research collaboration fund of Samsung Advanced Institute of Technology (SAIT) and JSPS KAKENHI Grant Number JP20H02374 and JP23H01626.

Ethical Approval: Not applicable.

Authors' contributions: T.S., H.Y., and M.O. wrote the main manuscript text, and T.S. and H.Y. prepared all figures. T.K., J.K., D.K., T.Y., and M.O. designed the plasma reactor and the experiment. All authors reviewed the measured data and the manuscript.

Availability of data and materials: The data and materials that support the findings of this study are available from the corresponding author upon reasonable request.

Conflicts of interest: The authors declare that they have no known competing financial interests or personal relationships that may have appeared to influence the work reported in this paper.

References

[1] Yamasaki H, Kishimoto K, Shimada T, Kuroki T, Kang J, Kim DW, Yagi T, Okubo M (2022) Toward ideal VOCs and nanoparticle emission control technology using a wet-type catalysis nonthermal plasma reactor. IEEE Trans Ind Applicat 58:6591–6598

[2] Shayegan Z, Haghighat F, Lee CS (2019) Photocatalytic oxidation of volatile organic compounds for indoor environment applications: Three different scaled setups. Chem Eng J 357:533–546

[3] Liotta LF (2010) Catalytic oxidation of volatile organic compounds on supported noble metals. Appl Catal B 100:403–412

[4] Xin Y, Ando Y, Nakagawa S, Nishikawa H, Shirai T (2020) New possibility of hydroxyapatites as noble-metal-free catalysts towards complete decomposition of volatile organic compounds. Catal Sci Technol 10:5453–5459

[5] Zhang X, Gao B, Creamer AE, Cao C, Li Y (2017) Adsorption of VOCs onto engineered carbon materials: A review. J Hazard Mater 338:102–123

[6] Cheng Y, He H, Yang C, Zeng G, Li X, Chen H, Yu GL (2016) Challenges and solutions for biofiltration of hydrophobic volatile organic compounds. Biotechnol Adv 34:1091–1102

[7] Urashima K, Chang JS (2000) Removal of volatile organic compounds from air streams and industrial flue gases by non-thermal plasma technology. IEEE Trans Dielectr Elect Insul 7:602–610

[8] Kohno H, Berezin AA, Chang JS, Tamura M, Yamamoto T, Shibuya A, Hondo S (1998) Destruction of volatile organic compounds used in a semiconductor industry by a capillary tube discharge reactor. IEEE Trans Ind Appl 34:953–966

[9] Oda T, Takahashi T, Yamaji K (2002) Nonthermal plasma processing for dilute VOCs decomposition. IEEE Trans Ind Appl 38:873–878

[10] Shibata T, Nishiyama H (2014) Acetic acid decomposition in a coaxial dielectric barrier discharge tube with mist flow. Plasma Chem. Plasma Process 34:1331–1343

[11] Kuroki T, Nishii S, Kuwahara T, Okubo M (2017) Nanoparticle removal and exhaust gas cleaning using gas-liquid interfacial nonthermal plasma. J Electrostat 87:86–92

[12] Takehana K, Kuroki T, Okubo M (2018) Evaluation on nitrogen oxides and nanoparticle removal and nitrogen monoxide generation using a wet-type nonthermal plasma reactor. J Phys D: Appl Phys 51:204002

[13] Yamasaki H, Nomura S, Xun X, Kuroki T, Kang J, Yagi T, Okubo M (2021) Toward NO_x/SO_x and nanoparticle control technology using a single-stage wet-type nonthermal plasma reactor. IEEE Trans Plasma Sci 49:1860–1870

[14] Yamamoto T, Ramanathan K, Lawless PA, Ensor DS, Newsome JR, Plaks N, Ramsey H (1992) Control of volatile organic compounds by an ac energized ferroelectric pellet reactor and a pulsed corona reactor. IEEE Trans Ind Appl 28:528–534

[15] Tonkyn RG, Barlow SE, Orlando TM (1996) Destruction of carbon tetrachloride in a dielectric barrier/packed-bed corona reactor. J Appl Phys 80:4877–4886

[16] Feng X, Liu H, He C, Shen Z, Wang T (2018) Synergistic effects and mechanism of a non-thermal plasma catalysis system in volatile organic compounds removal: a review. Catal Sci Technol 8:936–954

[17] Kim HH, Teramoto Y, Negishi N, Ogata A (2015) A multidisciplinary approach to understand the interactions of nonthermal plasma and catalyst: A review. Catal Today 256:13–22

[18] Futamura S, Yamamoto T (1997) Byproduct identification and mechanism

determination in plasma chemical decomposition of trichloroethylene. IEEE Trans Ind Appl 33:447–453

[19] Wang B, Chi C, Xu M, Wang C, Meng D (2017) Plasma-catalytic removal of toluene over CeO_2-MnO_x catalysts in an atmosphere dielectric barrier discharge. Chem Eng Sci 322:679–1692

[20] Yao X, Zhang J, Liang X, Long C (2018) Plasma-catalytic removal of toluene over the supported manganese oxides in DBD reactor: Effect of the structure of zeolites support. Chemosphere 208:922–930

[21] Kim HH, Abdelaziz AA, Teramoto Y, Nozaki T, Hensel K, Mok YS, Saud S, Nguyen DB, Lee DH, Kang WS (2021) Interim report of plasma catalysis: Footprints in the past and blueprints for the future. Int J Plasma Environ Sci Technol 15:e01004

[22] Ogata A, Shintani N, Yamanouchi K, Mizuno K, Kushiyama S, Yamamoto T (2000) Effect of water vapor on benzene decomposition using a nonthermal-discharge plasma reactor. Plasma Chem Plasma Process 20:453–467

[23] Gunten UV (2003) Ozonation of drinking water: Part I. Oxidation kinetics and product formation. Water Research 37:1443–1467

[24] Patil BS, Cherkasov N, Lang J, Ibhadon AO, Hessel V, Wang Q (2016) Low temperature plasma-catalytic NO_x synthesis in a packed DBD reactor: Effect of support materials and supported active metal oxides. Appl Catal B: Environ 194:123–133

[25] Chen HL, Lee HM, Chen SH, Chang MB (2008) Review of packed-bed plasma reactor for ozone generation and air pollution control. Ind Eng Chem Res 47:2122–2130

[26] Kishimoto K, Kumazawa Y, Kuroki T, Yamasaki H, Okubo M (2020) Ultrasonically

enhanced electrohydraulic discharge for removal of organic compounds. J Electrostat 108:103502

[27] Madhukar A, Rajanikanth BS (2019) Cascaded Plasma–Ozone Injection System: A novel approach for controlling total hydrocarbon emission in diesel exhaust Plasma Chem Plasma Process 39:845–862

[28] Hosseini H, Ghaffarzadeh M (2022) Investigation of plasma induced reactions of liquid toluene in Ar/NH_3: the formation of organic compounds through radical intermediates. Chem Lett 51:784–787

[29] Satoh K, Nagao K, Itoh H (2012) Decomposition characteristics of benzene, toluene and xylene in an atmospheric pressure DC corona discharge I. Characteristics of gaseous by-products. Trans Mat Res Soc Japan 37:151−155

[30] Shoukat H, Altaf AA, Hamayun M, Ullah S, Kausar S, Hamza M, Muhammad S, Badshah A, Rasool N, Imran M (2021) Catalytic oxidation of toluene into benzaldehyde and benzyl alcohol using molybdenum-incorporated manganese oxide nanomaterials. ACS Omega 6:19606−19615

[31] NIST Chemical Kinetics Database. https://kinetics.nist.gov/kinetics/ (accessed on 1 May 2023)

[32] Mizushima T, Thach TTC, Wen WJ, Ohkita H (2021) Tubular membrane-like catalysts for the oxidative decomposition of low-concentrated toluene in air by periodic short-term plasma discharge. Plasma Chem Plasma Process 41:607–617

[33] Ye Z, Veerapandian SK, Onyshchenko I, Nikiforov A, De Geyter N, Giraudon JM, Lamonier JF, Morent R (2017) An in-depth investigation of toluene decomposition with a glass beads-packed bed dielectric barrier discharge reactor. Ind Eng Chem Res 56:10215–10226

[34] Huang H, Ye D, Leung DYC, Feng F, Guan X (2011) Byproducts and pathways of toluene destruction via plasma-catalysis. J Mol Catal A Chem 336:87–93

[35] Tahara M, Okubo M (2014) Detection of free radicals produced by a pulsed electrohydraulic discharge using electron spin resonance. J Electrostat 72:222–227

[36] National Institute of Standards and Technology. https://webbook.nist.gov/chemistry/form-ser/ (accessed on 14 June 2022)

[37] The National Institute of Advanced Industrial Science and Technology. https://sdbs.db.aist.go.jp/sdbs/cgi-bin/cre_index.cgi/ (accessed on 14 June 2022)

[38] Kosaka K (2011) Ozone reactions in water. Chemical Education, 59:74–77 (in Japanese)

[39] Yamasaki H, Mizuguchi Y, Nishioka R, Fukuda Y, Kuroki T, Yamamoto H, Okubo M (2022) Pilot-scale NO_x and SO_x aftertreatment by semi-dry plasma-chemical hybrid process in glass-melting-furnace exhaust gas. Plasma Chem Plasma Process 42:51−71

Figure and Table Captions

All color figures are preferably color on the Web only.

Fig. 1 Schematic of the wet-type packed-bed nonthermal plasma reactor

Fig. 2 Schematic of the experimental setup

Fig. 3 Waveforms of the voltage V, current I, and instantaneous power $V \times I$ for the plasma reactor

Fig. 4 Particle-size distribution of nanoparticles introduced into reactor at the inlet without solution flow and plasma application

Fig. 5 Partial collection efficiency for nanoparticles at an NaOH solution flow rate of q = 75 mL/min with plasma application

Fig. 6 Relationship between the toluene removal efficiency and *SE* with various solution flow rates, NaOH solution concentrations, and initial concentrations at a pulse frequency of f = 840 Hz with a gas flow rate of Q = 10 L/min

Fig. 7 Relationship between the concentration of ozone at the reactor outlet and *SE* with various solution flow rates, NaOH solution concentrations, and initial toluene concentrations at a pulse frequency of f = 840 Hz with a gas flow rate of Q = 10 L/min

Fig. 8 FTIR spectra of the byproducts with various NaOH solution concentrations at a pulse frequency of f = 840 Hz with a solution flow rate of q = 100 mL/min and a gas flow

rate of Q = 10 L/min; (a) NaOH = 0, (b) NaOH = 0.31 mmol/L, (c) NaOH = 2.5 mmol/L, (d) NaOH = 6.25 mmol/L

Table 1 Toluene removal efficiencies, and O_3, CO, and CO_2 concentrations for various experimental conditions of NaOH solution concentrations

Fig. 9 Relationship between the toluene removal efficiency and *SE* with various pellet sizes at a pulse frequency of f = 210 Hz with gas flow rates of Q = 4 and 10 L/min and tap water flow rates of q = 0 and 100 mL/min

Fig. 10 Relationship between the ozone concentration and *SE* at the reactor outlet at a pulse frequency of f = 210 Hz with gas flow rates of Q = 4 and 10 L/min and tap water flow rates of q = 0 and 100 mL/min

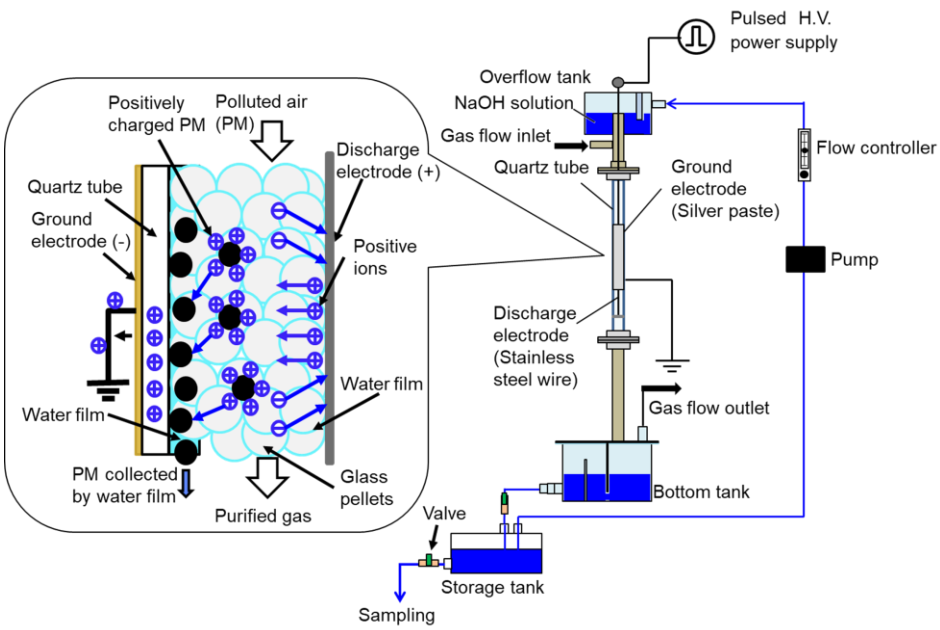
Positively charged PM
Polluted air (PM)
Discharge electrode (+)
Quartz tube
Ground electrode (-)
Positive ions
Water film
Water film
PM collected by water film
Glass pellets
Purified gas
Pulsed H.V. power supply
Overflow tank
NaOH solution
Gas flow inlet
Quartz tube
Ground electrode (Silver paste)
Flow controller
Pump
Discharge electrode (Stainless steel wire)
Gas flow outlet
Bottom tank
Valve
Storage tank
Sampling

Fig. 1

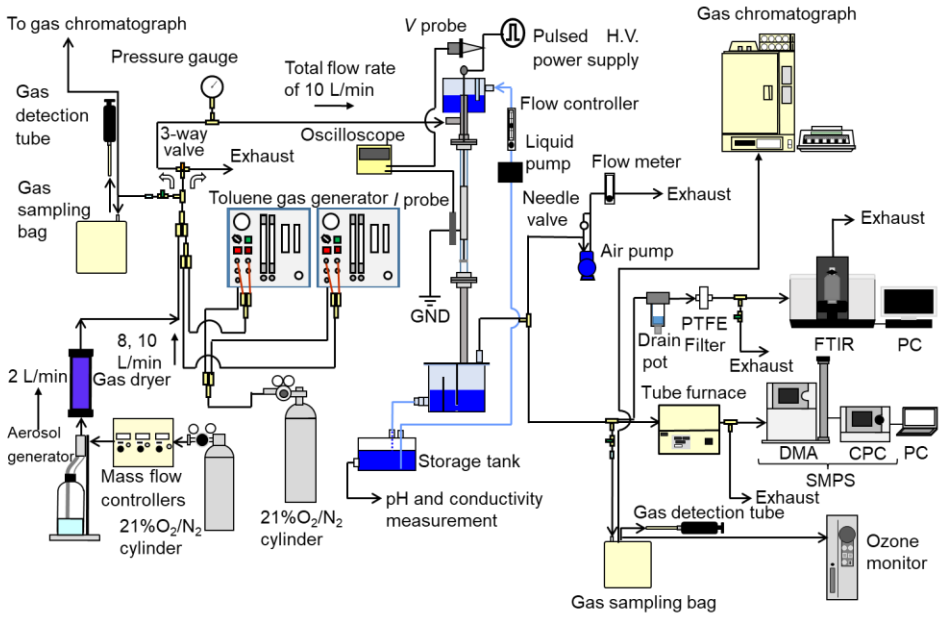
To gas chromatograph
Pressure gauge
Total flow rate of 10 L/min
V probe
Pulsed power supply
H.V.
Gas chromatograph
Gas detection tube
3-way valve
Exhaust
Oscilloscope
Flow controller
Liquid pump
Flow meter
Gas sampling bag
Toluene gas generator / probe
Needle valve
Exhaust
Air pump
Exhaust
GND
PTFE Filter
Drain pot
Exhaust
FTIR
PC
8, 10 L/min
2 L/min
Gas dryer
Tube furnace
Aerosol generator
DMA
CPC
PC
SMPS
Mass flow controllers
Storage tank
Exhaust
Gas detection tube
21%O2/N2 cylinder
21%O2/N2 cylinder
pH and conductivity measurement
Ozone monitor
Gas sampling bag

Fig. 2

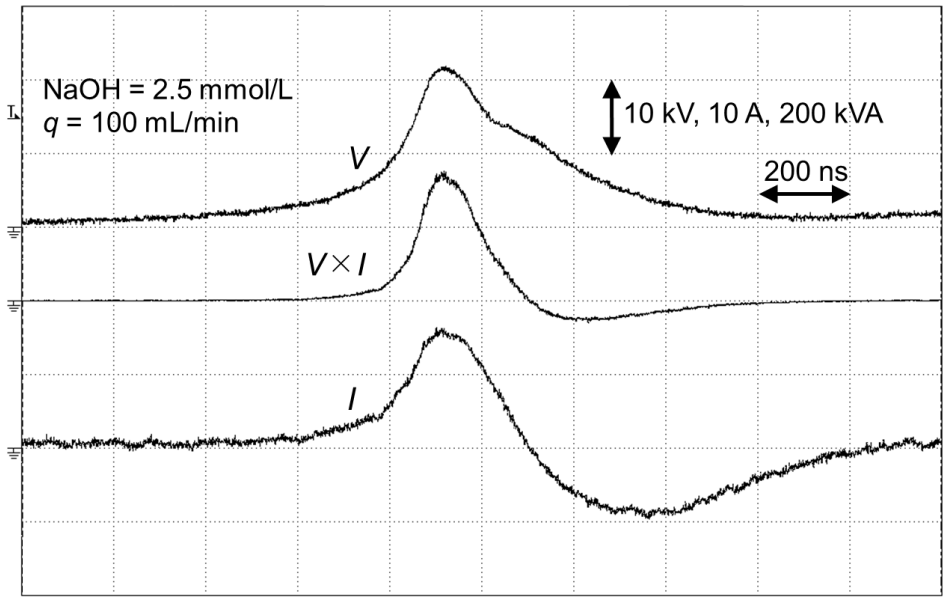

Fig. 3

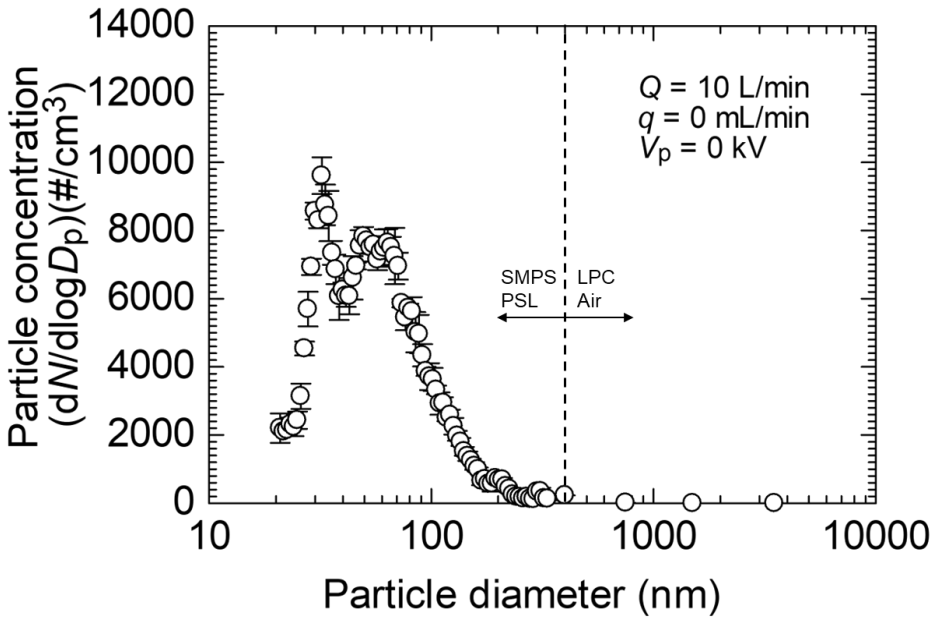
Particle concentration
(dN/dlogD_p)(#/cm^3)
14000
12000
10000
8000
6000
4000
2000
0
10
100
1000
10000
Particle diameter (nm)
Q = 10 L/min
q = 0 mL/min
V_p = 0 kV
SMPS
PSL
LPC
Air

Fig. 4

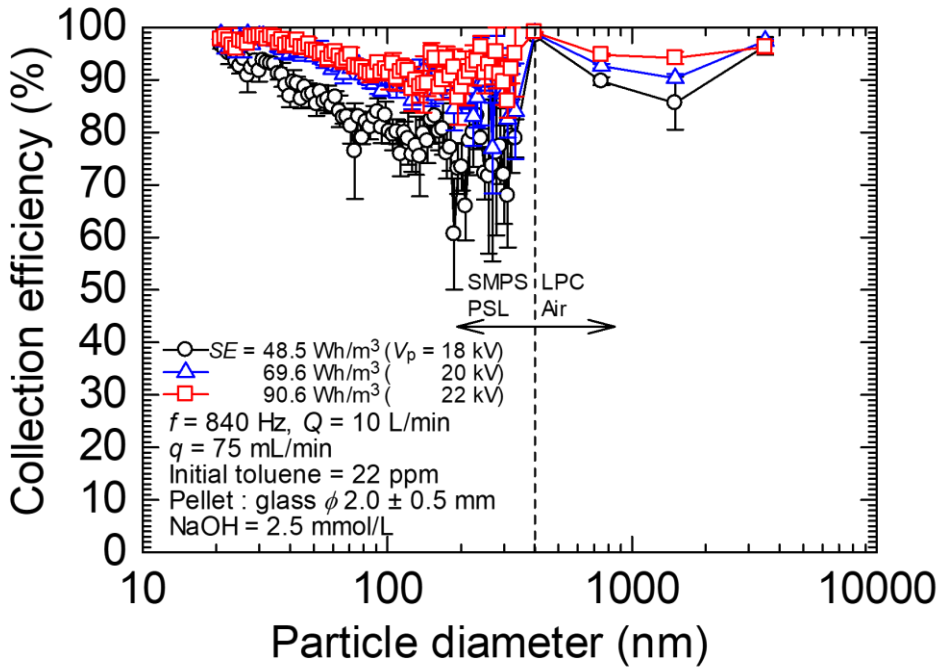
Collection efficiency (%)
100
90
80
70
60
50
40
30
20
10
0
10
100
1000
10000
Particle diameter (nm)
SMPS
LPC
PSL
Air
SE = 48.5 Wh/m3 (Vp = 18 kV)
69.6 Wh/m3 (20 kV)
90.6 Wh/m3 (22 kV)
f = 840 Hz, Q = 10 L/min
q = 75 mL/min
Initial toluene = 22 ppm
Pellet : glass ϕ 2.0 ± 0.5 mm
NaOH = 2.5 mmol/L

Fig. 5

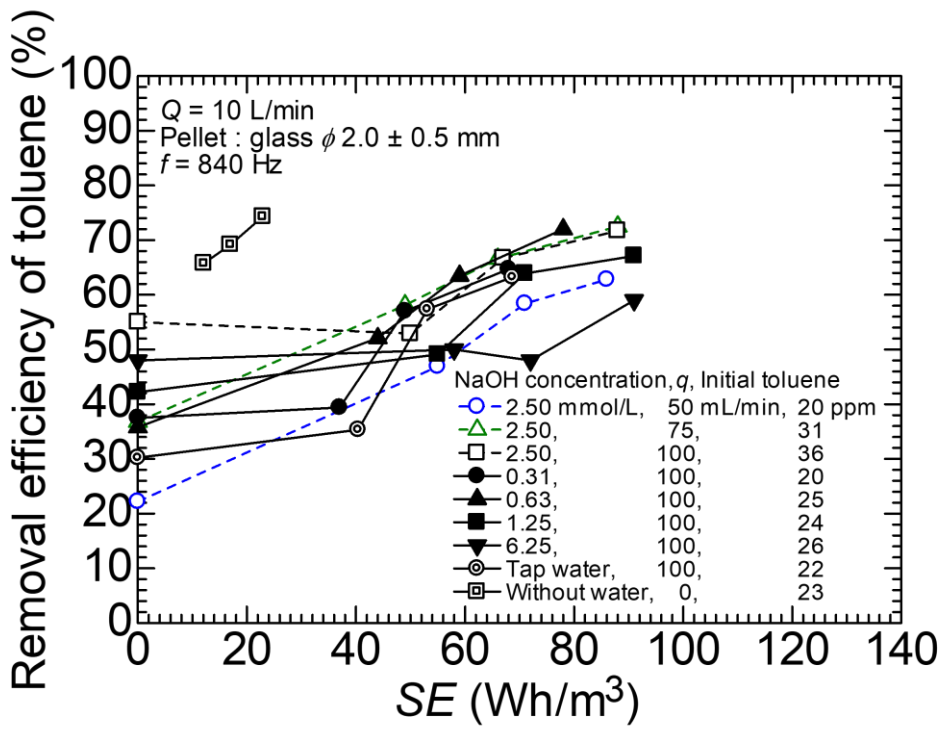
Q = 10 L/min
Pellet : glass ϕ 2.0 ± 0.5 mm
f = 840 Hz
NaOH concentration, q, Initial toluene
2.50 mmol/L, 50 mL/min, 20 ppm
2.50, 75, 31
2.50, 100, 36
0.31, 100, 20
0.63, 100, 25
1.25, 100, 24
6.25, 100, 26
Tap water, 100, 22
Without water, 0, 23
Removal efficiency of toluene (%)
SE (Wh/m3)
0
10
20
30
40
50
60
70
80
90
100
0
20
40
60
80
100
120
140

Fig. 6

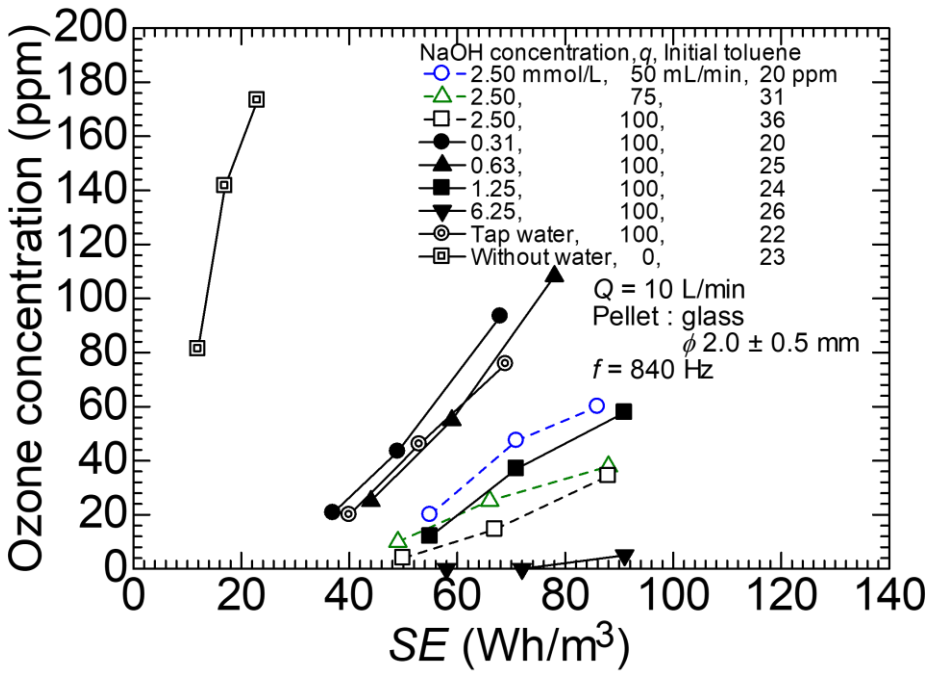
NaOH concentration, q, Initial toluene
2.50 mmol/L, 50 mL/min, 20 ppm
2.50, 75, 31
2.50, 100, 36
0.31, 100, 20
0.63, 100, 25
1.25, 100, 24
6.25, 100, 26
Tap water, 100, 22
Without water, 0, 23
Q = 10 L/min
Pellet : glass
ϕ 2.0 ± 0.5 mm
f = 840 Hz
Ozone concentration (ppm)
SE (Wh/m3)
0
20
40
60
80
100
120
140
160
180
200

Fig. 7

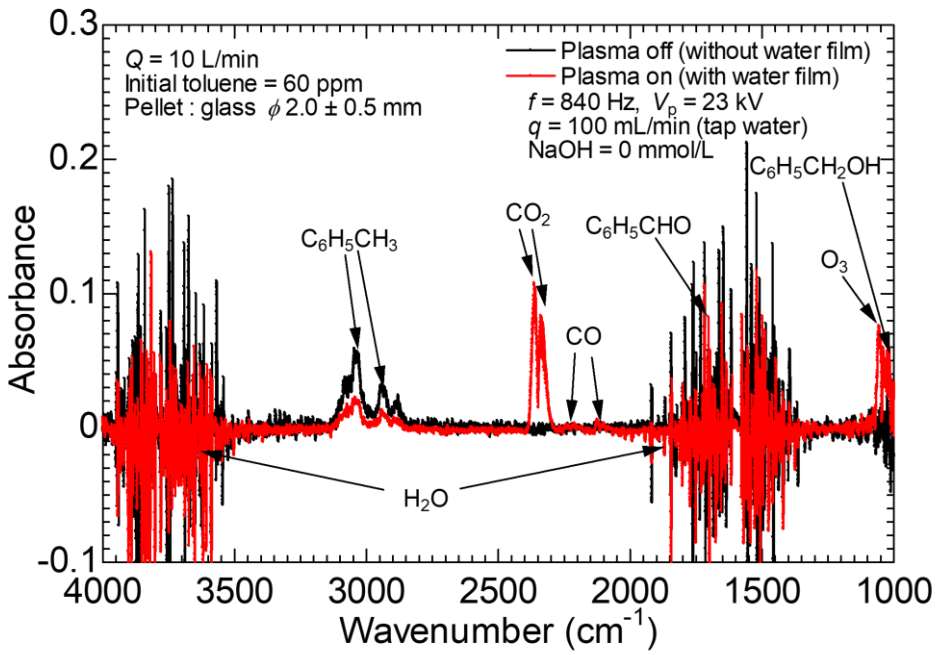
Q = 10 L/min
Initial toluene = 60 ppm
Pellet : glass ϕ 2.0 ± 0.5 mm
Plasma off (without water film)
Plasma on (with water film)
f = 840 Hz, V_p = 23 kV
q = 100 mL/min (tap water)
NaOH = 0 mmol/L
C6H5CH3
CO2
C6H5CHO
CO
C6H5CH2OH
O3
H2O
Absorbance
Wavenumber (cm-1)
0.3
0.2
0.1
0
-0.1
4000
3500
3000
2500
2000
1500
1000

Fig. 8(a)

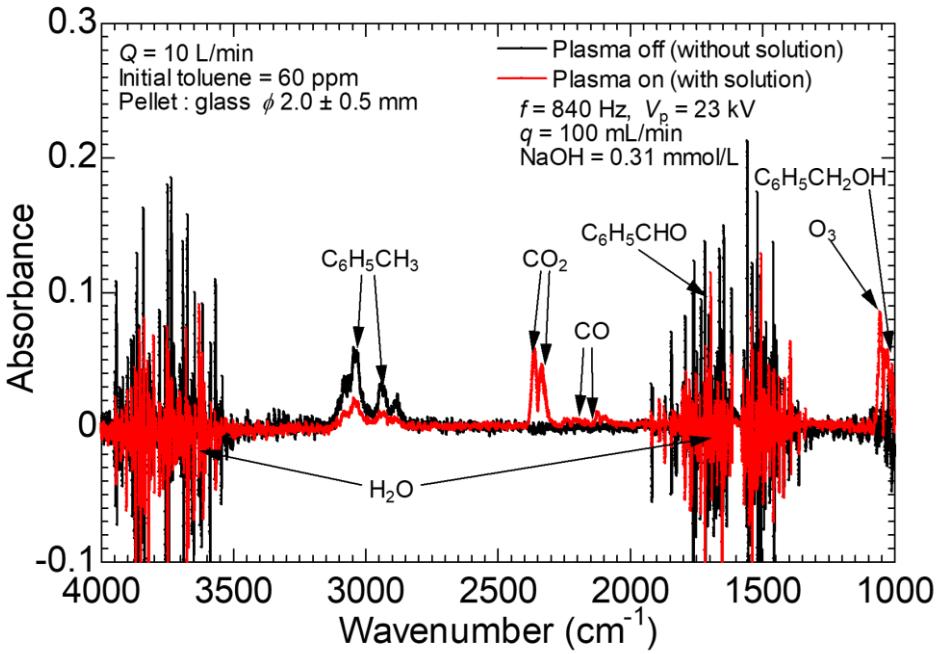
Q = 10 L/min
Initial toluene = 60 ppm
Pellet : glass ϕ 2.0 ± 0.5 mm
Plasma off (without solution)
Plasma on (with solution)
f = 840 Hz, V_p = 23 kV
q = 100 mL/min
NaOH = 0.31 mmol/L
C6H5CH3
CO2
C6H5CHO
CO
C6H5CH2OH
O3
H2O
Absorbance
Wavenumber (cm-1)
0.3
0.2
0.1
0
-0.1
4000
3500
3000
2500
2000
1500
1000

Fig. 8(b)

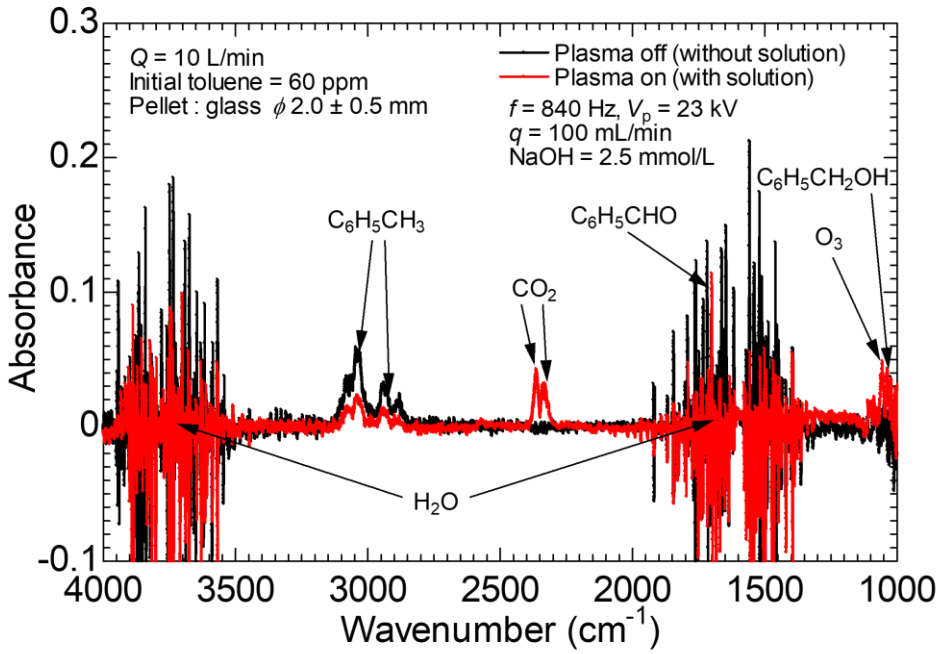
Q = 10 L/min
Initial toluene = 60 ppm
Pellet : glass ϕ 2.0 ± 0.5 mm
Plasma off (without solution)
Plasma on (with solution)
f = 840 Hz, V_p = 23 kV
q = 100 mL/min
NaOH = 2.5 mmol/L
C6H5CH3
CO2
C6H5CHO
O3
C6H5CH2OH
H2O
Absorbance
Wavenumber (cm-1)
0.3
0.2
0.1
0
-0.1
4000
3500
3000
2500
2000
1500
1000

Fig. 8(c)

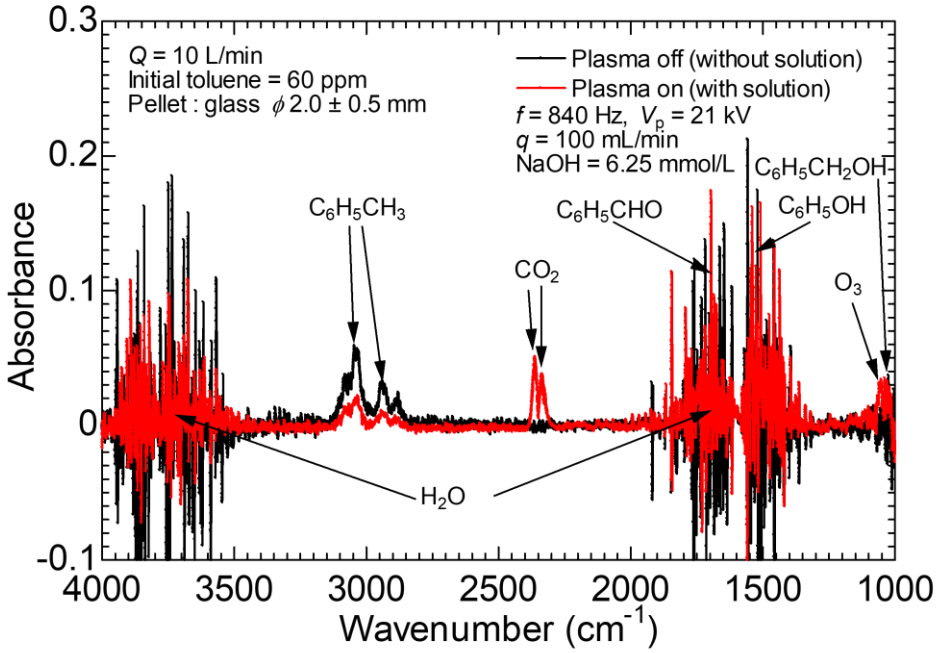
Q = 10 L/min
Initial toluene = 60 ppm
Pellet : glass ϕ 2.0 ± 0.5 mm
Plasma off (without solution)
Plasma on (with solution)
f = 840 Hz, V_p = 21 kV
q = 100 mL/min
NaOH = 6.25 mmol/L
C6H5CH3
C6H5CHO
C6H5CH2OH
C6H5OH
CO2
O3
H2O
Absorbance
Wavenumber (cm-1)
0.3
0.2
0.1
0
-0.1
4000
3500
3000
2500
2000
1500
1000

Fig. 8(d)

Table 1

Fig. 8	NaOH solution concentration mmol/L	Initial average concentration ppm	Discharge power W	Removal efficiency %	O_3 concentration ppm	CO_2 concentration ppm	CO concentration ppm
(a)	0	22	41	63	76	36	27
(b)	0.31	20	41	65	93	20	18
(c)	2.5	36	53	73	34	13	0
(d)	6.25	26	55	59	5	15	0

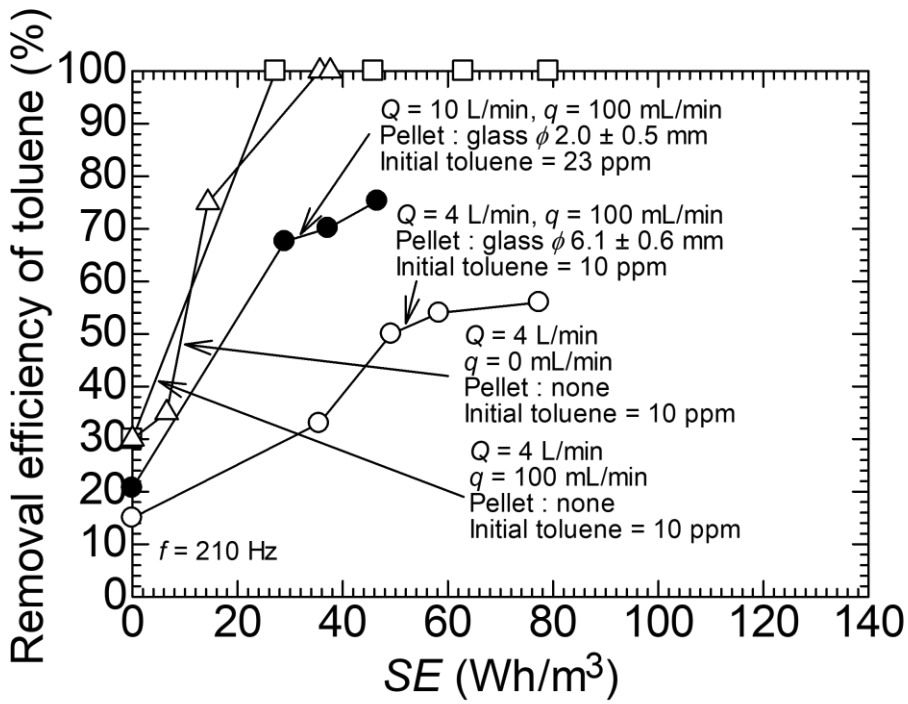
Removal efficiency of toluene (%)
100
90
80
70
60
50
40
30
20
10
0
0
20
40
60
80
100
120
140
SE (Wh/m3)
Q = 10 L/min, q = 100 mL/min
Pellet : glass ϕ 2.0 ± 0.5 mm
Initial toluene = 23 ppm
Q = 4 L/min, q = 100 mL/min
Pellet : glass ϕ 6.1 ± 0.6 mm
Initial toluene = 10 ppm
Q = 4 L/min
q = 0 mL/min
Pellet : none
Initial toluene = 10 ppm
Q = 4 L/min
q = 100 mL/min
Pellet : none
Initial toluene = 10 ppm
f = 210 Hz

Fig. 9

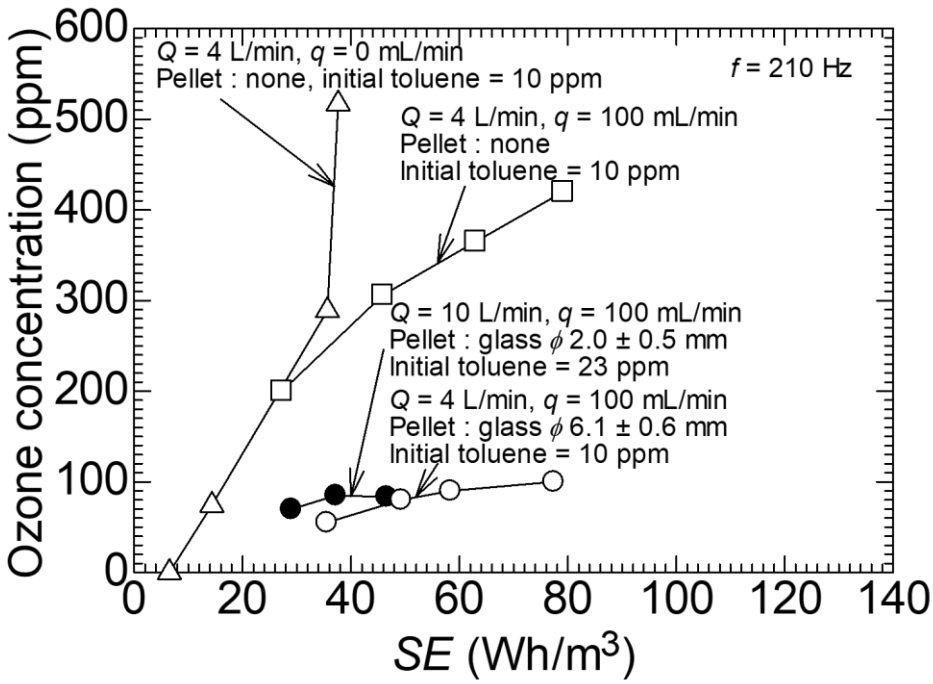
Ozone concentration (ppm)
600
500
400
300
200
100
0
0
20
40
60
80
100
120
140
SE (Wh/m3)
Q = 4 L/min, q = 0 mL/min
Pellet : none, initial toluene = 10 ppm
f = 210 Hz
Q = 4 L/min, q = 100 mL/min
Pellet : none
Initial toluene = 10 ppm
Q = 10 L/min, q = 100 mL/min
Pellet : glass ϕ 2.0 ± 0.5 mm
Initial toluene = 23 ppm
Q = 4 L/min, q = 100 mL/min
Pellet : glass ϕ 6.1 ± 0.6 mm
Initial toluene = 10 ppm

Fig. 10